Waveform Analysis of Acoustic Emission in Concrete

By

Yoshiji NIWA*, Masayasu OHTSU** and Hiroyuki SHIOMI***

(Received May 9, 1981)

Abstract

In order to utilize AE phenomena in materials research and for nondestructive testings, considerable basic studies are urgently required in order to clarify the physical meanings of AE signals.

For this end, extensive studies in correlations between AE parameters and mechanical behaviors of concrete materials and structures have been carried out in our research.

In this paper, some of our recent developments on AE waveform analysis are described. In searching for the source mechanisms of AE, the aim of waveform analysis may be to separate the effects of the propagation media and the transducers from the detected AE waveforms, and to determine the kinetic and kinematic characteristics of sources. Therefore, the deconvolution techniques in both the time domain and the frequency domain are developed. They have been applied to investigate two basic types of sources, namely, a point force and a tensile crack.

Results show that our original notions concerning the source mechanisms of AE, which can be mathematically described by the dislocation model, are acceptable. The applicability of elastodynamics and the dislocation theory for studying the relation between the source mechanisms and wave motions of AE is also verified.

1. Introduction

Acoustic Emission[1], which is abbreviated as AE, is the transient elastic wave emission that is spontaneously released when materials undergo deformation, fracture, or both. It is considered that AE phenomena can offer attractive potentialities for monitoring the structural integrity[2] and for characterizing mechanical behaviors in materials. Intensive studies[3] have been carried out in correlations between AE signals and the mechanical behaviors of concrete structures.

While industrial AE applications and instrumentation developments have progressed well in recent years[4], precise interpretations of waveforms and sources still have some

* Department of Civil Engineering
** Department of Civil Engineering
(Present address: Kumamoto University)
*** Department of Civil Engineering
(Present address: Kyoto Prefecture Government)

problems. In order to clarify the mechanisms responsible for AE in rock-like materials such as concrete and rock, where the creation and running of cracks are proposed as major sources[5], an analysis of AE wave motions is required as a matter of course. Generally, the phenomena of wave motions have been analyzed in either the frequency domain or the time domain. It can be mathematically shown that the representations in the two domains are equivalent. The analytical difficulties in both domains lie in the lack of understanding the source mechanisms, the wave propagation details, and the precise physical meanings of the transducer mechanical-electrical conversion process.

In the frequency domain, the AE signal flow process can be considered as the linear system[6], where the original source spectra are multiplied at each frequency by the frequency response of the propagation media, the transducer, and other electronics. The calibrated spectra by the frequency response of the transducer and detecting system have been investigated in respect to the location and type of sources[7].

In the time domain analysis, it has been known that AE waveforms could be simulated by postulating the mathematical model based on the theory of dislocation and elastodynamics[8], where AE wave motions were related to Green's function and the source time function by a convolution integral.

In the following, the theory of waveform analysis is discussed and the deconvolution techniques are developed. AE waveforms generated by two basic types of sources, which are referred to as a point force and a tensile crack in the dislocation theory, are detected in the half space model specimens of mortar and concrete. They are simulated theoretically. Then, the source time functions are determined by the deconvolution techniques, which analyze wave motions in either the time domain or the frequency domain.

2. Theory

AE phenomena are defined as the elastic wave emissions due to some faulting in a solid. From this point of view, the source characterization of AE may not be much different from the focal mechanism of an earthquake. In other words, earthquakes are another AE phenomena on a global scale.

One of the most elegant approaches to the problem of modelling an earthquake is the Knopoff-de Hoop representation theorem[9].

If the representation theorem is applied to the dynamic dislocation in a homogeneous and isotropic medium, it can be shown that the resulting displacement at any ponit is written in the following form[8]

$$u_m(\boldsymbol{x}, t) = \int_{-\infty}^{\infty}\int_{\Sigma} \{T_{mi}(\boldsymbol{x}, t-t'; \boldsymbol{\xi}) [u_i(\boldsymbol{\xi}, t')] + G_{mi}(\boldsymbol{x}, t-t'; \boldsymbol{\xi}) f_i(\boldsymbol{\xi}, t')\} d\boldsymbol{\xi} dt' \qquad (2\text{-}1)$$

where $[u_i]$ is the discontinuity in displacement components which is specified over the fault surface $\sum$, f_i is the equivalent force by which the effect of discontinuity in strsse can be described[10], and G_{mi} is Green's function, which represents the displacement in the m-direction at $(\boldsymbol{x}, t)$ due to an instantaneous point force of unit impulse in the i-direction at $(\boldsymbol{\xi}, t')$. Note that T_{mi} indicates such combinations of partial derivatives of G_{mi} with respect to the source coordinates $\boldsymbol{\xi}$'s as follows:

$$T_{mi}=\lambda G_{mk,k'}\nu_i+\mu(G_{mi,j'}+G_{mj,i'})\nu_j \tag{2-2}$$

where ν_i is the unit normal to the surface $\sum$, and λ and μ are the Lamé constants.

If the area of the surface $\sum$ in equation (2-1) is regarded as infinitesimal compared with the surrounding body, and the displacement field is an elastodynamic state with a quiescent past[11], then the surface integral is evaluated only at the source point $\boldsymbol{\xi}$. Then, the equation (2-1) becomes

$$u_m(\boldsymbol{x}, t)=\int_0^t\{T_{mi}(\boldsymbol{x}, t-t';\boldsymbol{\xi})[u_i(\boldsymbol{\xi}, t')]+G_{mi}(\boldsymbol{x}, t-t';\boldsymbol{\xi})f_i(\boldsymbol{\xi}, t')\}dt'. \tag{2-3}$$

It follows that the displacement component u_m is related with the resultant effects of the discontinuity in displacement and a point force, which are defined as the dislocations at the source.

The elastic waves travel from the source within the medium and are picked up as AE on the boundary, where the surface tractions vanish. Therefore, in equation (2-3), the solution at a free surface is required for the problem of the elastic displacements resulting from the dislocations in a half space.

The problem of determining the elastic disturbance resulting from a point force in a half space is known as Lamb's problem. Then, Green's function G_{mi} is the solution of Lamb's problem for the delta function time dependency force. It can be calculated numerically by using the programs provided for both cases of forces, which are the surface pulse[12] and the buried pulse[13].

The spatial derivatives of G_{mi} are also evaluated in the same manner[13], and T_{mi} in equation (2-3) can be obtained from equation (2-2).

From equation (2-3), the sources are separated into two cases. The one is a point force which is namely Lamb's problem. The other is the dislocation in displacement which has been generally considered as the governing mechanism of fracture.

In both cases, it has been already known that the physical quantities of AE waveforms detected through our system can be admittedly assumed as vertical accelerations[8].

Considering the half space with $x_3=0$ defining the free surface and positive x_3 pointing toward the half space as shown in Fig. 1, equation (2-3) becomes Lamb's problem and the dislocation in displacement respectively,

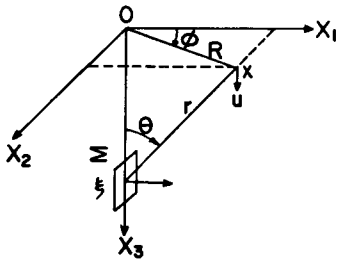

Fig. 1. Geometry of the dislocation surface Σ in a half space.

$$\ddot{u}_3(t) = \int_0^t G_{3i}(t-t')\,\ddot{f}_i(t')\,dt' \qquad (2\text{-}4)$$

$$\ddot{u}_3(t) = \int_0^t T_{3i}(t-t')\,[\ddot{u}_i(t')]\,dt' \qquad (2\text{-}5)$$

where a dot indicates the time derivative, and the detecting point $\boldsymbol{x}$ at a free surface and the source point $\boldsymbol{\xi}$ are evaluated implicitly, since they are not correlated directly to a convolution integral.

Once the sources, about which some informations in regard to the kinetics and kinematics are known, are represented by the time functions, the AE waveforms can be simulated by either equation (2-4) or (2-5). Inversely, because the transient wave propagation behaviors of a half space are known, unknown sources can be characterized as the time functions through deconvolution.

Then both equations (2-4) and (2-5) belong to a class of linear integral equations of the Volterra type of the first kind, where the source time functions $f_i(t)$ and $[u_i(t)]$ are unknown. The concept of deconvolution or the analysis of the integral equation has been investigated[14], and the detailed procedures are discussed later.

3. Experiment

The specimens, which were used as the half space model in this study, are plates with dimensions being $6 \times 30 \times 30$ cm. They are made of mortar and concrete with mix proportions, respectively, water: cement: sand = 0.6: 1.0: 2.0, and water: cement: sand: gravel = 0.64: 1.0: 2.0: 4.0, with a maximum gravel size of 10 mm. These compressive strengths and velocities of the *P*-wave were 32 Mpa, 3900 m/sec for mortar and 31.2 Mpa, 4400 m/sec for concrete at twenty-eight days.

A block diagram of the monitoring and recording system is shown in Fig. 2. Basically, the monitoring system consists of the commercial piezoelectric transducer 905*S* (resonant frequency 1 MHz), a band pass filter, and an amplifier unit set with a 60 dB total gain. A frequency range is selected for 10 kHz-300 kHz.

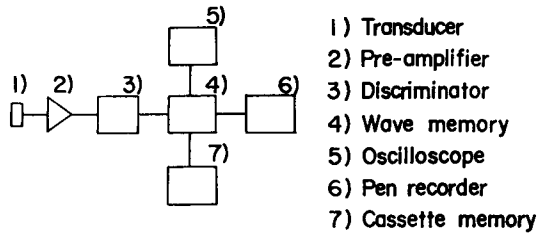

Fig. 2. Block diagram of the AE monitoring and recording system.

AE signals are relatively short duration transients (a few msec [10^{-3}sec]), which often contain frequency components distributed over a very wide range. The system for recording such transients must be accurate, introduce the least possible distortion, and facilitate further analysis of the recorded data.

Consequently, the recording system, which consists of the wave memory and the digital cassette tape unit, was used. The output signals of the monitoring system are fed into the wave memory and recorded at a 50 nsec [10^{-9}sec] sampling time, after which the data are logged onto the digital cassette tape unit.

In experiments, AE waveforms generated by two types of the source mechanisms were detected. One was a point force corresponding to Lamb's problem, and the other was a tensile crack, which was the discontinuity in displacement component parallel with the unit normal to the fault surface.

The experimental configuration for the surface pulse of Lamb's problem is shown in Fig. 3. The point force was produced at the center of the upper surface by the piezoelectric transducer, into which the electric step pulse was driven. AE waveforms at the point of E, as shown, were detected and recorded by the above-mentioned system. For the case of the buried pulse, the point force was produced at the center of the opposite surface.

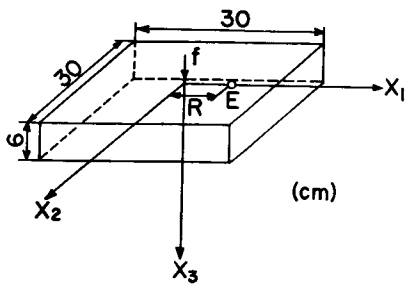

Fig. 3. Sketch of the experiment for the surface pulse of Lamb's problem.

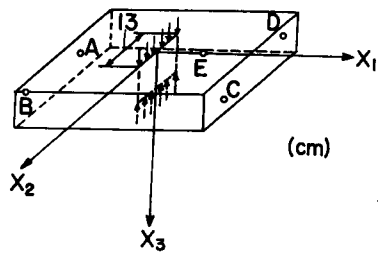

Fig. 4. Sketch of the split test, generating tensile cracks in the half space model specimen.

A sketch of the split test is shown in Fig. 4. As the line load increased gradually, generated AE waveforms were detected at the point of E and also recorded onto the digital cassette tape. At the same time, the source location system[15] consisting of the transducers A, B, C, and D was applied and the sources were located. In this experiment, it was supposed that the tensile cracks were generated in the potential plane of failure, near the x_2-x_3 plane between the line loads. Therefore, the sources, which were not located on this plane approximately, were omitted.

After the tests had been completed, the data were read from the tape unit, and

transmitted via the time sharing terminal to the large computer (FACOM M200 in data processing center), and then stored on a disk. The computer program was used for the waveform analysis and for plotting the results.

4. Result and Discussion

As to an appropriate choice of $f(t)$ for Lamb's problem in this experiment, it has been discussed and already known[8] that the form of $f(t)$ starts with a zero slope, approaches smoothly to a peak, and remaihs constant, which can be assumed as follows:

$$df(t)/dt=\sin^4(\pi t/T_r) \quad (0\leqq t\leqq T_r). \qquad (4\text{-}1)$$

The appearance of $f(t)$ in the case of $T_r=10$ μsec, together with that of df/dt in equation (4-1) and d^2f/dt^2 required for a convolution integral in equation (2-4), are shown in Fig. 5.

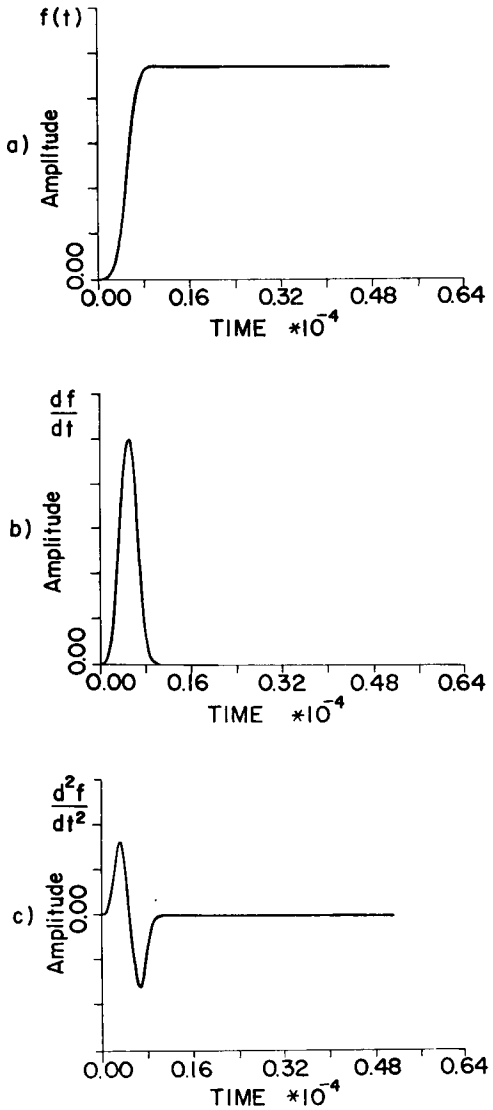

Fig. 5. Assumed source waveform for $T_r=$ 10 μsec in equation (4-1).

Although the derivaton of Green's function is based on the problem for a half space, the solution is perfectly applicable to such a finite plate as shown in Fig. 3 within a finite period. This period corresponds to a first arrival of the ray reflected from the opposite side of the plate.

By reducing an integration in equation (2-4) into a finite summation as a sampling interval of Δt and denoting

$$\ddot{u}(I)=\ddot{u}_3(I\Delta t);$$
$$\ddot{f}(I)=\ddot{f}_3(I\Delta t);$$
$$G(I)=G_{33}(I\Delta t)\,\Delta t,$$

equation (2-4) can be written as

$$\ddot{u}(I)=\sum_{K=1}^{I}G(I-K+1)\,\ddot{f}(K) \quad (I=1, 2, \ldots\ldots, N). \qquad (4\text{-}2)$$

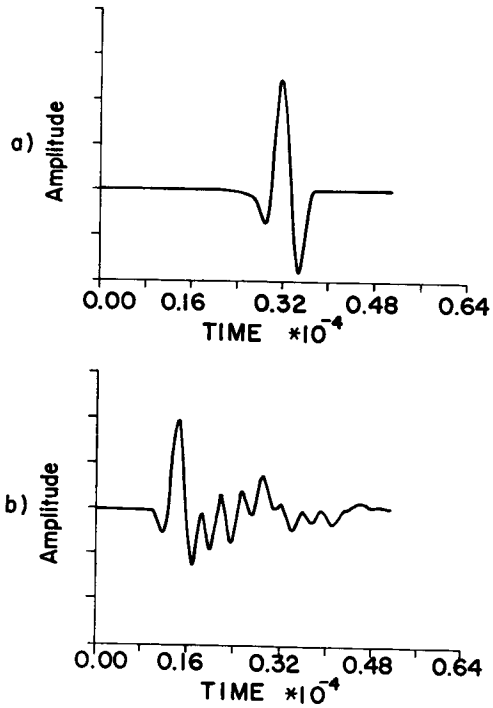

Fig. 6. AE waveforms for the surface pulse of Lamb's problem in mortar, a) simulated and b) detected for R= 6 cm.

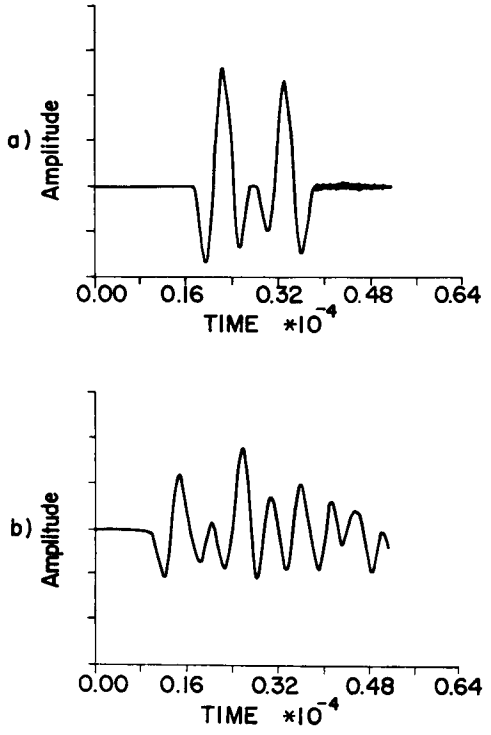

Fig. 7. AE waveforms for the buried pulse of Lamb's problem in mortar, a) simulated and b) detected for R=3 cm.

An example of the simulated AE waveforms by equation (4-2) and those detected by the preceding system for the surface pulse of Lamb's problem is shown in Fig. 6. The physical quantities of the vertical axis are accelerations in Fig. 6 a) and electric voltages in Fig. 6 b). Since the precise ratio of electrical-mechanical conversion is unknown, the vertical scales are relative in both. The time duration before the initial part of the wave motions in Fig. 6 a) corresponds to a theoretical arrival time. However such a duration is meaningless in Fig. 6 b), because it was not known when the AE signal was triggered by the wave memory. A fairly good agreement between the computed vertical acceleration and the detected AE waveform can be shown within a limited period after the first arrival.

The comparison between the simulated and detected waveforms for the buried pulse of Lamb's problem is shown in Fig. 7. A good correlation is also shown in most respects of the initial part of wave motions.

These results confirm that the solution for a half space is applicable to the spe-

cimen in this study, and provide a rational basis to determine the source time function through deconvolution procedures.

Thus, equation (4-2) may be looked upon as a system of linear algebraic equations solving the unknown $\ddot{f}(I)$.

It is easy to see that $\ddot{f}(I)$ can be solved successively by simple substitution and division, i.e.

$$\ddot{f}(1) = \ddot{u}(1)/G(1)$$
$$\ddot{f}(I) = [\ddot{u}(I) - \sum_{K=1}^{I-1} G(I-K+1)\,\ddot{f}(K)]/G(1) \qquad (I=1, 2, \ldots, N) \qquad (4\text{-}3)$$

In calculating the deconvolution by means of equation (4-3), the number $G(1)$ occurs repeatedly in the denominators of the $\ddot{f}(I)$ terms. It can be expected that if $G(1)$ is small, the numbers $\ddot{f}(I)$ become large as I increases and they oscillate at the same time. However, if $G(1)$ is large compared with the other values of $G(I)$, then $\ddot{f}(I)$ will not be divergent as I increases.

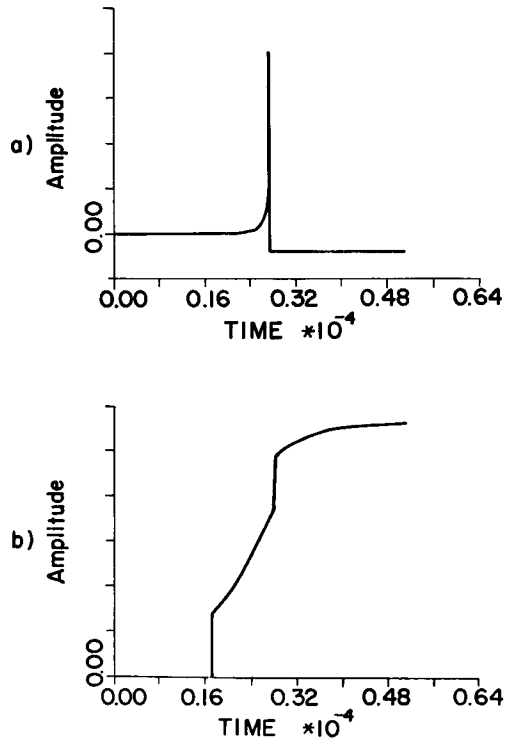

Fig. 8. Theoretical waveforms of G_{33}, a) for the surface pulse in the case of Fig. 6, and b) for the buried pulse in the case of Fig. 7, which result from the source with a step-function time dependency.

In Green's function of Lamb's problem, the solution for the surface pulse may belong to the former case, and the buried pulse to the latter case. Green's functions in the cases of Fig. 6 and Fig. 7 are shown in Fig. 8. These solutions result from the source which is a step function in time and are used for the deconvolution procedures by integrating equation (4-3) with respect to time. It shows that $G(1)$, which is the beginning part of the curve which is not equal to zero, for the surface pulse is even smaller than the other value of $G(I)$, but rather large for the buried pulse.

From these results, the applicability of equation (4-3), which hereafter will be called the time domain deconvolution, to the buried pulse problem has been examined. The solid curve shown in Fig. 9 is obtained by the time domain deconvolu-

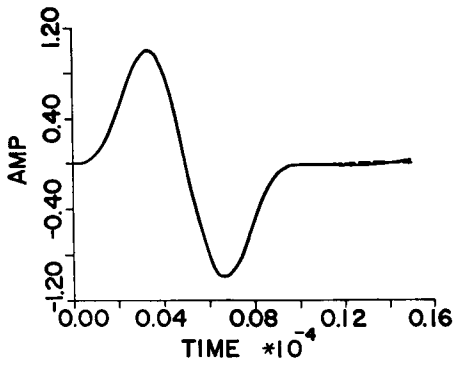

Fig. 9. Source waveforms of d^2f/dt^2 for the buried pulse of Lamb's problem. The solid curve is obtained by the time domain deconvolution of the curve in Fig. 7 a), and the dashed curve is the same as the assumed waveform shown in Fig. 5 c).

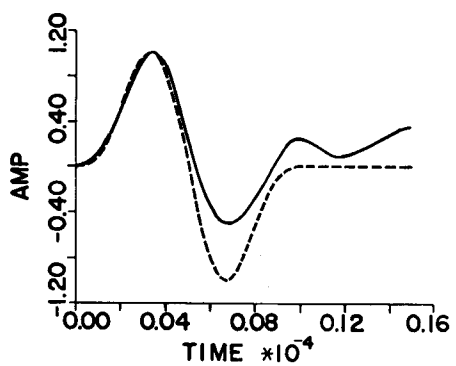

Fig. 10. Source waveforms of d^2f/dt^2 for the buried pulse of Lamb's problem. The solid curve is obtained by the time domain deconvolution of the curve in Fig. 7 b), and the dashed curve is the same as shown in Fig. 9.

tion of the curve in Fig. 7 a) and the dashed curve is the same as that of the assumed, as shown in Fig. 5 c). They are normalized with the first peak amplitude. The agreement shows that the source time function for the buried pulse can be determined with precision and numerical stability by the time domain deconvolution.

The procedure was applied to the detected AE waveform shown in Fig. 7 b) and the result is shown in Fig. 10. The source time function calculated from the experimental data actually resembles the assumed function. It becomes clear that the response of the transducer 905S, which is generated by driving the electric step pulse, can be represented approximately by equation (4-1), and T_r is equal to about 10 μsec. Also, it is considered that the acceptability of the simulation analysis[8] is verified consistently.

In the case of the surface pulse problem, the preceding result shows that the alternative method for a deconvolution must be required. It is known that in the frequency domain, a convolution integral corresponds to a multiplication, and the frequency spectrum of the source time function is obtained by simple division

$$\bar{F}_3(f) = \bar{G}_{33}(f) / \bar{U}_3(f) \tag{4-4}$$

where $\bar{F}_3$, $\bar{G}_{33}(f)$, and $\bar{U}_3(f)$ are the Fourier transforms of $f_3(t)$, $G_{33}(t)$, and $u_3(t)$ respectively. Equation (4-4) may be the counterpart of the time domain deconvolution in the frequency domain. Then $\bar{f}_3(t)$ can be obtained by the inverse Fourier transform to the time domain.

This procedure, which hereafter will be called the frequency domain deconvolu-

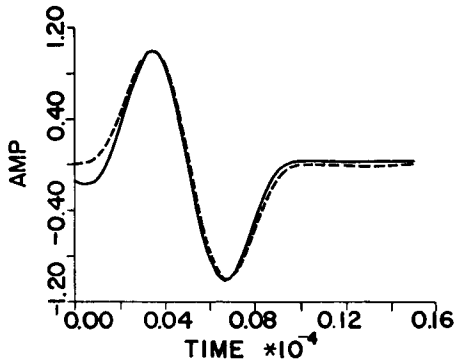

Fig. 11. Source waveforms of d^2f/dt^2 for the surface pulse of Lamb's problem. The solid curve is obtained by the frequency domain deconvolution of the curve in Fig 6 a), and the dashed curve is the same as the assumed shown in Fig. 5 c).

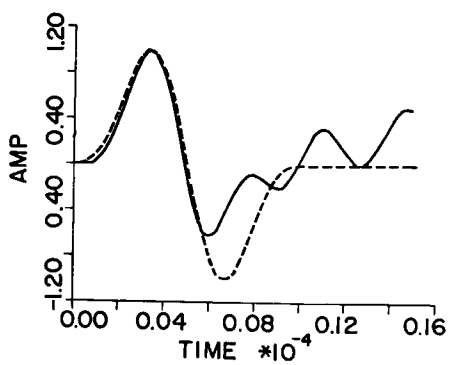

Fig. 12. Source waveforms of d^2f/dt^2 for the surface pulse of Lamb's problem. The solid curve is obtained by the frequency domain deconvolution of the curve in Fig. 6 b), and the dashed curve is the same as shown in Fig. 11.

tion, has been developed and applied to the surface pulse problem. The result, which has been obtained from the calculated curve in Fig. 6 a), is shown in Fig. 11. The computer program based on the fast Fourier transform was used for calculating equation (4-4) and the inverse transformation. The initial part of the computed source time function shifts slightly from that of the assumed curve by the linking effect of the discrete Fourier transform. A very good correlation between the computed and the assumed is shown, and the applicability of the frequency domain deconvolution to the surface pulse problem is also verified.

The result, which has been obtained by the frequency domain deconvolution of the detected AE waveform in Fig. 6 b), is shown in Fig. 12. The initial part of the computed function is in good agreement with that of the assumed. The remaining part, however, differs from the assumed curve, and does not look like that of such a time function for the buried pulse, as shown in Fig. 10. Considering that the path of the ray reflected from the opposite side of the specimen cannot reach the transducer within these periods, it may be due to possible calculating errors or smoothing effects produced by the finite size of the transducer, because the AE signal is integrated over the area of the electrode of the transducer.

In the split test, AE waveforms, sources of which were located near the potential plane of failure previously described, were detected. A tensile crack was considered as the discontinuity in the x_1-direction displacement components, which was parallel to the unit normal to such a fault plane on the x_2-x_3 plane, as shown in Fig. 4. Equation (2-5) follows from equation (2-2) as

$$\ddot{u}_3(t) = \int_0^t T_{31}(t-t')\,[\ddot{u}_1(t')]\,dt' \tag{4-5}$$

$$T_{31} = (\lambda+2\mu)G_{31,\,1}' + \lambda G_{32,\,2}' + \lambda G_{33,\,3}'$$

The comparison between the simulated AE waveform based on equation (4-5) and the detected one is shown in Fig. 13. In this simulation analysis, $[\ddot{u}_1(t)]$ in equation (4-5) is assumed to be the same as $f(t)$ shown in Fig. 5. T_r is determined so that the simulated waveform fits the detected one as well as possible.

The transfer function T_{31} in equation (4-5), which results from the tensile crack source with a step-function time dependency, is shown in Fig. 14. The location of the source is denoted in the caption of Fig. 13.

It shows that the frequency domain deconvolution suits this problem. The computed source time function $[\ddot{u}(t)]$, which has been obtained by the frequency

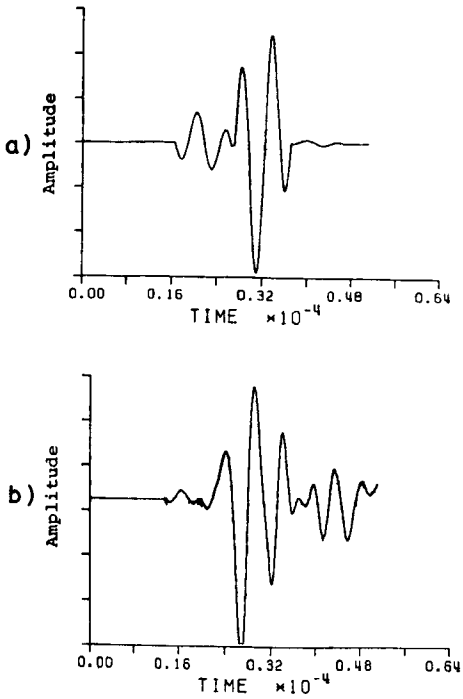

Fig. 13. AE waveforms, a) simulated and b) detected for the tensile crack source in concrete. The source coordinate is (0.2, -1.3, 4.2) in Fig. 4 and $T_r = 10$ μsec.

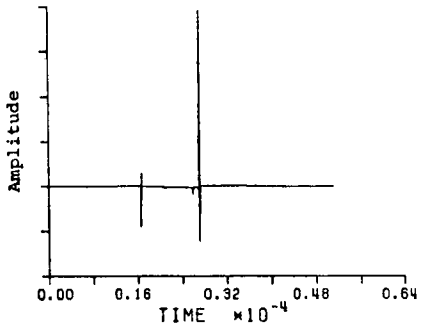

Fig. 14. Theoretical waveform of T_{31}. The location of the source, which is a step function in time, is denoted in the caption of Fig. 13.

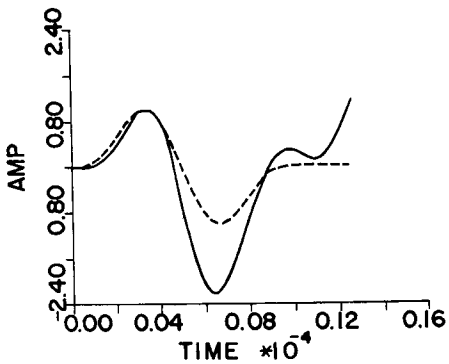

Fig. 15. Source waveforms for the split test. The solid curve is obtained by the frequency domain deconvolution of the curve in Fig. 13, and the dashed curve is the assumed source waveform. Both curves represent $[\ddot{u}(t)]$.

domain deconvolution of the detected waveform in Fig. 13 b), is shown in Fig. 15. A good agreement between the computed and the assumed for the period shown is obtained.

It is confirmed that our original notions concerning the source mechanism of AE, which can be mathematically described by the dislocation model, are acceptable. The agreement also verifies the applicability of elastodynamics and the dislocation theory for studying the relation between the source mechanisms and wave motions of AE.

5. Conclusion.

In this paper, theoretical representations of AE waveforms in concrete materials have been studied and verified by experiments. In searching for the source mechanisms of AE, the aim of waveform analysis may be to separate the effects of the propagation media and the transducers from the detected AE waveforms, and then to determine the kinetic and kinematic characteristics of sources. The analytical tools for characterizing the propagation media are their representations, which are transfer functions or Green's function in the time domain, and spectra in the frequency domain. The deconvolution techniques in both domains are developed. They have been applied to investigate the sources, which are a point force and a tensile crack, and wave motions of AE are clarified to a certain degree. It is also suggested that AE is a promising method for observing the microscopic dynamic deformation process itself in concrete.

References

1) Liptai, R.G. et al.; "Acoustic Emission", ASTM STP 505, (1972).
2) Spanner, J.C. and J.W. McElroy et al.; "Monitoring Structural Integrity by Acoustic Emission", ASTM STP 571, (1975).
3) Niwa, Y., S. Kobayashi and M. Ohtsu; Proc. Jap. Soc. Civ. Engrs., No. 261 (1977).
4) Hartman, W.F. and J.W. McElroy et al.; "Acoustic Emission Monitoring of Pressurized Systems", ASTM STP 697, (1979).
5) Hardy, Jr., H.R. and F.W. Leighton et al.; "Proceedings 2nd Conference on Acoustic Emission/Microseismic Activity in Geologic Structures and Materials", Trans Tech Publications (1977).
6) Pao, Y.H.; "Elastic Waves and Non-Destructive Testing of Materials", AMD-**29**, ASME (1978).
7) Niwa, Y., S. Kobayashi, M. Ohtsu and K. Okuda; Proc. Jap. Soc. Civ. Engrs., No. 314 (1981).
8) Niwa, Y., S. Kobayashi and M. Ohtsu; Proc. Jap. Soc. Civ. Engrs., No.314 (1981).
9) Burridge, R. and L. Knopoff; Bull. Seism. Soc. Amer., **54** (1964).
10) Maruyama, T.; Bull. Earthq. Res. Inst., **41** (1963).
11) Eringen, A.C. and E.S. Suhubi; "Elastodynamics, Volume II Linear Theory", Academic Press (1975).
12) Mooney, H.M.; Bull. Seism. Soc. Amer., **64** (1974).
13) Johnson, L.R.; Geophys. J.R. astr. Soc., **37** (1974).
14) Ko, H. and R.F. Scott; Bull. Seism. Soc. Amer., **57** (1967).
15) Niwa, Y., S. Kobayashi and M. Ohtsu; Proc. Jap. Soc. Civ. Engrs., No.276 (1978).